Influence of the Co-Condensation of Water and n-Heptane on Top of the Line Corrosion

Thunyaluk Pojtanabuntoeng,[‡,,**] Maryam Eslami,[*] Marc Singer,[*] and Srdjan Nešić[*]*

Top of the line corrosion (TLC) is a serious concern in wet gas transportation pipelines operating in a stratified flow regime. Extensive research on TLC has been conducted in hydrocarbon-free environments while, in production environments, condensable hydrocarbons are always present. When water and hydrocarbons co-condense, the condensate comprises two immiscible liquids which have different wettability and corrosivity. In this study, the co-condensation process was investigated using a borescope for visual observation and a set of conductivity probes for quantification of water-wetted area. The corrosion behavior of carbon steel under water-only condensation and water/hydrocarbon co-condensation scenarios was evaluated with weight loss measurements and surface analytical techniques (scanning electron microscopy, energy dispersive spectroscopy, and 3D profilometry). The results showed that water and hydrocarbon condensation processes interacted with each other. Even though the rate of hydrocarbon condensation was much greater than that of water, the hydrophilicity of the steel surface always ensured that it would be mainly wetted by water. However, the presence of n-heptane interfered with the water droplet coalescence and segregated water into smaller droplets which affected the water chemistry. This resulted in a potentially higher pH and iron ion concentration in the water droplet as compared to a water-only scenario. The corrosion rate consequently decreased and was found to be less dependent on the water condensation rate in the co-condensation scenario, as compared to a pure water system.

KEY WORDS: carbon steel, CO_2 corrosion, hydrocarbons, n-heptane, top of the line corrosion

INTRODUCTION

Top of the line corrosion (TLC) can pose a serious concern in stratified wet gas transmission pipelines. TLC failure was first reported in the 1960s and several other field cases have subsequently been published.[1-3] The temperature difference between the inside and outside of the pipe results in the condensation of water vapor on the internal surface of the pipe wall. This condensed water found at the top of the line can be considerably more corrosive than the water accumulated at the bottom of the line as it has a lower pH and is not buffered by the presence of formation water. Additionally, the injection of corrosion inhibitors, which may successfully prevent corrosion at the bottom of the pipe, is not effective against TLC because the flow regime does not allow ready transportation of the chemicals to the top portion of the internal pipe wall.

Extensive research has been conducted and key parameters influencing TLC have been investigated, e.g., condensation rate, temperature, pressure of acid gases, total pressure, presence of volatile organic acids, etc.[4-11] Gunaltun and Larrey noticed the direct correlation between water condensation rate (WCR) and TLC damage in several field cases and proposed that WCR is the primary controlling parameter.[7] High-WCR enhances the replenishing rate of freshly condensed liquid and prevents the formation of protective iron carbonate.[4,12] Gas and external temperature strongly govern TLC as the driving force for the rate of water condensation.[7] Anuar, et al.,[8] performed TLC-simulated experiments in a specifically designed glass cell at different condensation rates (0.02 g/m^2/s, 0.06 g/m^2/s, and 0.09 g/m^2/s). They observed the partial formation of $FeCO_3$ at all condensation rates tested and an increase in the number of pits with the condensation rate. Qian and Cheng[11] established a relationship between the thickness of water film on the specimen and the CO_2 corrosion rate. According to their results, the CO_2 corrosion rate increases with the thickness of the water layer. This is because with the increase in the thickness of the water layer, the formation of a protective iron carbonate becomes more challenging.

Several TLC prediction models, ranging from empirical to mechanistic, have been developed[13-15] but the possibility of hydrocarbon co-condensation had not been taken into account even by one of the most advanced models developed by Zhang, et al.[15] This is due to the lack of experimental investigation into this particular phenomenon. The vast majority of earlier TLC-related research focused on hydrocarbon-free systems even if, in production environments, the condensation of hydrocarbons often takes place concurrently with water. When that occurs, the condensed liquid comprises two immiscible liquids: one corrosive (water) and the other noncorrosive (hydrocarbon), having different surface wetting behavior.

At the bottom of the line, the effect of hydrocarbons on CO_2 corrosion has been widely investigated in two major aspects, i.e., corrosion inhibition by hydrocarbons[16] and water-wetting in multiphase flow.[17] The former is usually attributed to the presence of surface-active compounds found in crude oil.[18] Light and condensable hydrocarbons that perhaps appear at the top of the line may not contain such compounds. Lotz, et al., reported that light alkanes, such as n-hexane to n-octane, did not provide corrosion protection when present at the bottom of

Submitted for publication: September 22, 2021. Revised and accepted: January 31, 2022. Preprint available online: January 31, 2022, https://doi.org/10.5006/3952.
‡ Corresponding author. E-mail: thunyaluk.pojtanabuntoeng@curtin.edu.au.
* Institute for Corrosion and Multiphase Technology, Chemical and Biomolecular Engineering, Ohio University, Athens 45701, Ohio.
** Curtin Corrosion Centre, WASM-MECE, Curtin University, Technology Park, Bentley, Western Australia 6102, Australia.

ISSN 0010-9312 (print), 1938-159X (online)

Table 1. *Composition of X65 Carbon Steel (the Balance is Fe)*

Element	Al	As	B	C	Ca	Co	Cr	Cu	Mn	Mo	Nb
Content (wt%)	0.032	0.008	0.001	0.13	0.002	0.007	0.14	0.131	1.16	0.16	0.017
Element	Ni	P	Pb	S	Sb	Si	Sn	Ta	Ti	V	Zr
Content (wt%)	0.36	0.009	<0.001	0.009	0.009	0.26	0.007	<0.001	<0.001	0.047	<0.001

the line together with water.[19] Simon, et al., obtained similar findings but emphasized that the frequency of water coming into contact with the steel and its residence time also determined corrosion rate.[20] This scenario bears many similarities to a co-condensation situation.

When two immiscible liquids co-condense, different condensation patterns can be observed depending on their surface tensions and condensation rates. Organic liquids, especially hydrocarbons, usually form a film covering the surface due to their low surface tension while water or liquids with higher surface tension generally condense as droplets, unless their condensation rate is high enough.[21-24] The co-condensation patterns influence the heat/mass transfer which determines the rate of co-condensation.[21-23,25] Several mathematical correlations for a heat transfer coefficient in the presence of two immiscible condensing liquids were proposed for various geometries of condensing surfaces.[21,26]

Though the aforementioned research work was not directly related to TLC, it can be postulated that the co-condensation of water and hydrocarbons could possibly change the condensation pattern occurring in pipelines and affect the condensation rate which is considered as the primary parameter in TLC. Pojtanabuntoeng, et al., have shown earlier that the water condensation rate decreased when n-heptane co-condensed because the heat transfer coefficient of the mixed liquids decreased.[27]

To explore the influence of hydrocarbon co-condensation on TLC, this study investigated an in situ co-condensation process of water and n-heptane (a representative hydrocarbon) on horizontal or slightly downward-inclined surfaces, which is a configuration seen in large wet gas transmission pipelines.

EXPERIMENTAL PROCEDURES

This study is separated into two sections. In the first part, the water condensation process with and without hydrocarbons was investigated, whereas the effect of co-condensation on corrosion rate was studied in the second part. n-Heptane was used as the co-condensable hydrocarbon representative. Specimens of carbon steel API 5L X65[†] were used in all experiments. The composition of the steel specimens was shown in Table 1.

2.1 | Condensation Process Observation

Visual observation—A conventional 2 L glass cell was filled with 1.5 L of the desired test solution (either water or a mixture of water and n-heptane) leaving approximately 5 cm top space between the bulk liquid interface and the top lid. The solution was then heated up to generate warm vapor between 30°C and 50°C. A thermocouple was placed in the gas phase, at the same level as the sample. CO_2 was bubbled continuously throughout the experiment. Once the desired vapor (gas) temperature was obtained, the steel specimen, previously polished with silicon carbide (SiC) abrasive papers up to 600 grit, was introduced into the system and flush-mounted to the top lid. During the experiment, the specimen was cooled using a thermoelectric cooler. The detail of the specimen assembly was presented in Figure 1. The specimen temperature was approximately 30°C. A borescope was then inserted into the cell to observe and record the ongoing condensation process on the steel specimen. The vapor and specimen temperatures were constantly monitored.

Conductivity measurements—As water and n-heptane were both transparent, differentiating each phase was challenging if one only relies on the visual observation. Therefore, an additional technique was required. The difference in electrical conductivity of water and hydrocarbons has been used previously to identify the phase wetting in oil-water two-phase flow.[28-29] A similar concept was used in the present work to distinguish the nature of the liquid condensing at the steel surface.

The conductivity probe was manufactured from a carbon steel rod with a diameter of 31.75 mm. It was drilled and filled with 20 epoxy-insulated stainless steel pins, as shown in a schematic diagram and the photograph in Figure 2. The conductivity of the liquid wetting each probe surface was measured simultaneously by applying a DC voltage (3.0 V) between the pin and the surrounding carbon steel surface. Condensed water typically shows relatively low conductivity, but the small amount of iron dissolved from the corrosion process increases its

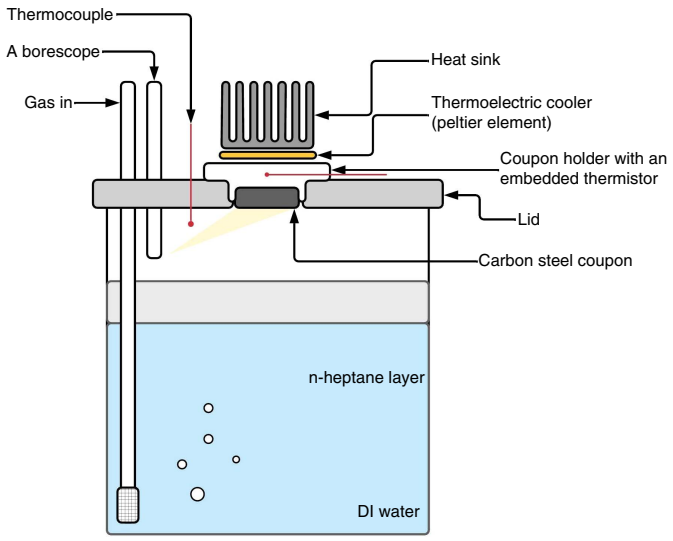

FIGURE 1. *Schematic drawing of setup used for the condensation observation experiments.*[27]

[†] Trade name.

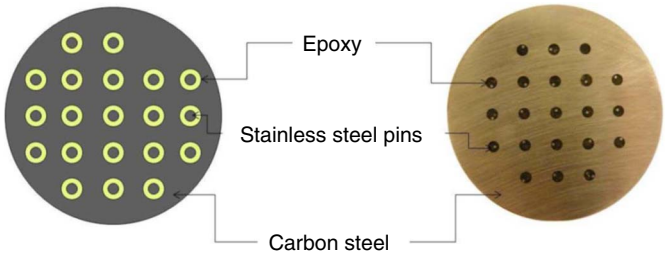

FIGURE 2. *Schematic diagram and the photograph of the conductivity probe.*

conductivity significantly. On the contrary, hydrocarbon always displays extremely high resistivity. Consequently, the nature of liquid wetting each pin was easily distinuguished. The percentage of surface area wetted with water was evaluated by counting the number of pins in contact with water.

The conductivity probe was polished up to 600 grit using SiC abrasive papers prior to testing to obtain similar surface roughness as a carbon steel specimen used in the visual observation experiments. The same glass cell setup, as described above, was used. After the vapor temperature attained a stable value, the conductivity probe was inserted in the cell and the change in the area wetted with water with respect to time was recorded. Because the cooling device could not be installed on the conductivity probe, the temperature difference between the vapor and probe surface was limited to approximately 2°C to 3°C in all cases.

2.2 | Corrosion Study

For the corrosion study, experiments were conducted in two different experimental setups in order to cover a wider range of flow conditions.

- In a glass cell setup with a stagnant condition, where a flat specimen was flush-mounted to the top of the lid and exposed to a relatively stagnant vapor phase, i.e., stagnant condition (Figure 1).
- In a flowing flow tube system where a cylindrical specimen was mounted in a 2.5 cm (1 in) tube and exposed to a flowing vapor phase, i.e., flowing vapor condition (Figure 3).

Stagnant condition—In this series of experiments, the electrolyte was sparged with CO_2 for at least 4 h. Subsequently,

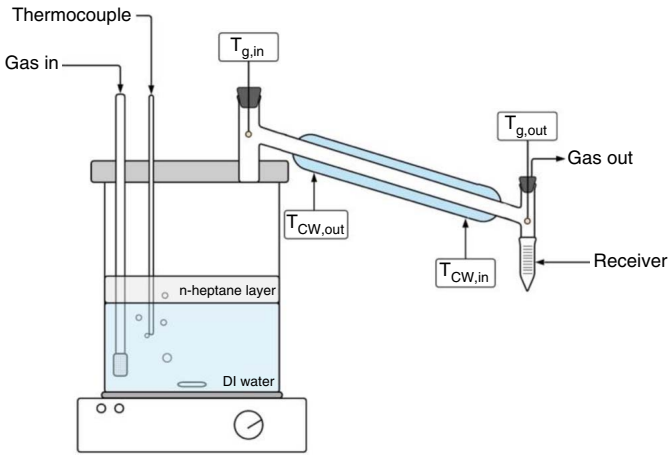

FIGURE 3. *Schematic diagram of the experimental setup for the corrosion test under a flowing condition.*

a steel specimen polished up to 600 grit SiC abrasive paper was inserted into the glass cell and exposed to the corrosive environment for 3 d and 13 d. As n-heptane would be depleted more quickly than water, deoxygenated n-heptane was added periodically during the experiment. The experimental parameters were described in Table 2. Each experiment was duplicated.

At the end of the experiment, the specimen was taken out, rinsed with deionized (DI) water and isopropanol, and air-dried. The specimen surface was characterized with scanning electron microscopy (SEM) and energy dispersive spectroscopy (EDS). Afterward, the specimen was cleaned with Clark's solution (20 g of Sb_2O_3 and 50 g of $SnCl_2$ in 1 L of 32 wt% HCl) to remove any corrosion product.[30] The corrosion rates were obtained from the weight loss measurements. The occurrence of localized corrosion was analyzed utilizing a 3D surface profilometry instrument.

Flowing vapor condition—A customized flow tube as shown in Figure 3 was used in this set of experiments to simulate flowing conditions. A conventional glass condenser with a cooling water jacket was adapted to hold a Teflon™† tube having an outside diameter of 1 in which served as a specimen holder. Two carbon steel specimens were mounted to the upper half at both ends of the tube. Water and n-heptane vapors saturated with CO_2 were generated in separate flasks. CO_2, which served as the corrosive gas as well as the carrier gas, was bubbled at a constant flow rate of 10 mL/s throughout the experiment. Temperature probes were positioned immediately below the carbon steel specimens to record the vapor temperature (T_v). The condensation rate was calculated by accounting for the difference in vapor pressure at the vapor and cooling water temperature (T_c). Details of the calculation and its validation with experimental results were previously presented.[31] Condensation rates were varied by adjusting the cooling water flow rate and temperature. Experiments duration was 1 d and 3 d. The experimental parameters and the calculated condensation rates of water and n-heptane were given in Table 2.

RESULTS AND DISCUSSION

3.1 | Condensation Process Monitoring

Visual observation—In the absence of n-heptane, water initially condensed as isolated droplets due to its high surface tension (Figures 4[a] and [b]). Adjacent drops grew, coalesced, and eventually formed a uniform film on the steel surface (Figures 4[c] and [d]). Water eventually accumulated as one single droplet and fell to the bottom of the cell when it reached its maximum size; the gravity force exceeded the surface tension and buoyancy force. This allowed freshly condensed water to occupy the same area (Figure 4[e]). At a higher WCR, the condensation also initiated as isolated drops, but the coalescence of nearby droplets proceeded more rapidly.

Figure 5 illustrates the co-condensation process of water and n-heptane. At a vapor temperature of 40°C and a cooling temperature of 27±2°C, the calculated condensation rate of water and n-heptane were 0.08 mL/m^2/s and 0.5 mL/m^2/s, respectively. Obviously, n-heptane condensed at a much faster rate compared to water. Isolated droplets were observed immediately (Figure 5[a]). n-Heptane, due to its low surface tension on the solid surface, tends to condense in a film-wise manner whereas water, due to its higher surface tension, condenses in a dropwise manner.[22] Therefore, it could be expected that the droplets would be comprised of water while

Table 2. *Test Matrix for Corrosion Experiments*

Parameters	Stagnant Condition		Flowing Condition	
	Water Condensation Only	Co-Condensation	Water Condensation Only	Co-Condensation
Material	X65			
Vapor Temperature (°C)	30–50	30–50	18–65	18–50
Cooling Temperature (°C)	25–30	25–30	–	–
Water Condensation Rate (mL/m^2/s)	0.06–0.22	0.05–0.19	0.001–0.6	0.001–0.15
n-Heptane Condensation Rate (mL/m^2/s)	–	0.33–1.21	–	0.001–1
Total Pressure (kPa)	101.3			

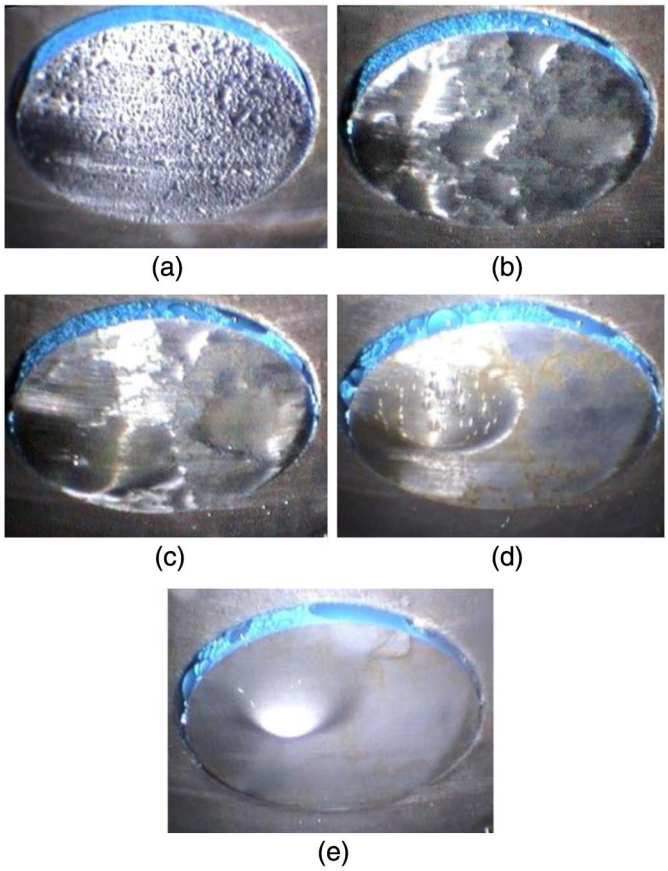

FIGURE 4. *Condensation behavior of water with time (T_v = 40±1°C, T_s = 30±2°C and WCR = 0.07±0.02 mL/m^2/s); (a) 5 min, (b) 10 min, (c) 45 min, (d) 1 h, and (e) >20 h.*

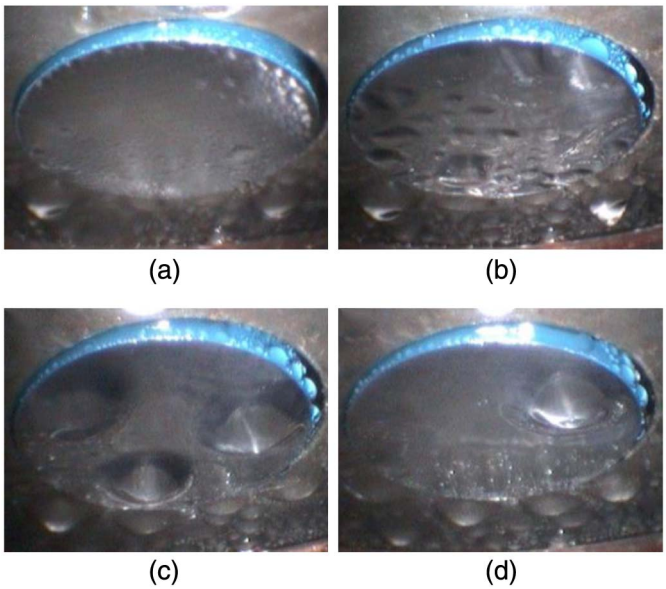

FIGURE 5. *The observation of co-condensation process with time. T_v = 40±1°C, cooling temperature = 27±2°C and condensation for water = 0.08±0.02 mL/m^2/s, for n-heptane = 0.5±0.15 mL/m^2/s; (a) 5 min, (b) 1 h, (c) 2.5 h, and (d) 4 h.*

the areas in between the droplets would be wetted with n-heptane. It was observed that the size of droplets increased with time indicating that they were water droplets that coalesced (Figures 5[b] and [c]). However, no further coalescence of those water droplets could be noticed after 3 h as the steel surface seemed to be covered with a liquid film. The coalescence of water droplets in co-condensation proceeded much more slowly than that in the pure water system, where surface wetting was fully obtained in less than 1 h. The co-condensation of n-heptane seemed to interfere with the droplet coalescence possibly due to the higher amount of n-heptane at the steel surface.

Nonetheless, at the end of co-condensation experiments, no phase distinction could be made by monitoring the process through a borescope, as can be seen in Figure 5(d). It was expected that water would gradually occupy the entire surface due to its stronger affinity for the carbon steel surface, i.e., carbon steel usually exhibits a hydrophilic behavior and therefore attracts water.[27,32] However, this could not be verified experimentally using only visual observation and an additional method based on electrical conductivity was used to monitor the condensation process and to confirm the presence of water at the steel surface.

3.1.1 | Results of the Electrical Conductivity Measurement

A preliminary condensation experiment was performed in pure water environment (no n-heptane) in order to characterize the probe response. Figure 6 shows an increase in the water-wetted area with time as the condensation of water progressed. The inset of Figure 6 demonstrates what happened during

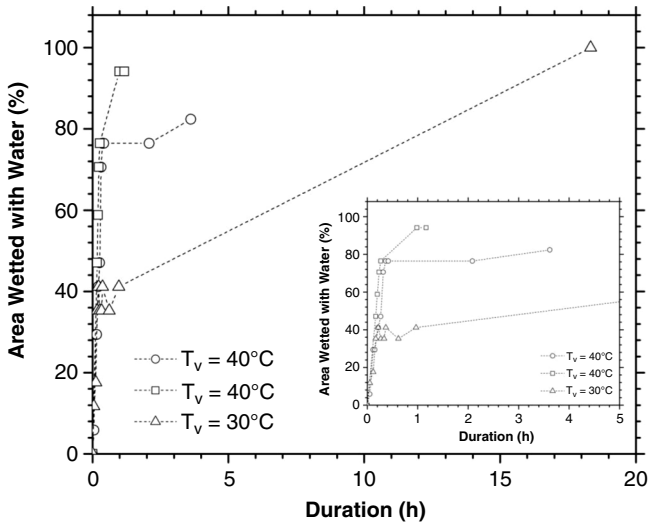

FIGURE 6. *Area fraction wetted with water vs. exposure time to water condensation from 0 h to 20 h and from 0 h to 5 h (inset).*

the first 4 h. At higher vapor temperature (T_v = 40°C), which corresponded to higher WCR, approximately 80% of the pins were covered with water within the first hour which is in agreement with the previous observations obtained with the borescope (Figure 4). At lower WCR, (T_v = 32°C), the coalescence proceeded more slowly, and less area was wetted with water in the first hour. Nonetheless, the gradual coalescence led to full surface coverage by water at the end of the experiment.

Figure 7 presents the water-wetted area in the co-condensation scenario at the same T_v of 40°C, hence under a slightly lower water condensation rate compared to the pure water environment.[27] The conductivity probe showed that water slowly occupied the surface, i.e., less than 50% of the specimen surface was wetted by water after 5 h of exposure. Water gradually occupied the whole surface and after 20 h water was clearly the dominant phase. This result provides a similar trend when compared to the results obtained with visual observation (Figure 5).

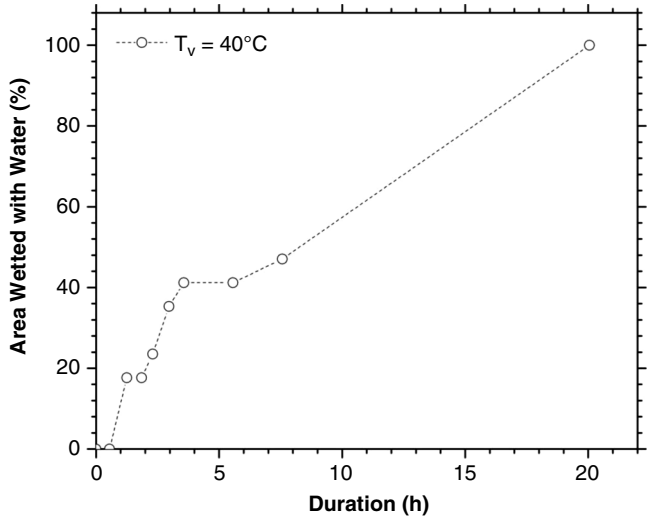

FIGURE 7. *Area fraction wetted with water with time in water and n-heptane co-condensation process. T_v = 40±2°C, ΔT = 3°C.*

In summary, two independent techniques were used to identify the liquids co-condensing at the steel surface and showed that water will eventually occupy the carbon steel surface regardless of the presence of n-heptane. This is due to the hydrophilic nature of carbon steel.[27]

3.2 | Corrosion Behavior

In the above-mentioned experiments, the results clearly show that water eventually wets the steel surface in all scenarios. Fast co-condensation of n-heptane did not prevent water from reaching the surface and corrosion remained a possibility. Therefore, the effect of co-condensation on corrosion was investigated and the main results are presented below. Corrosion experiments were conducted for two different exposure times, 3 d and 2 weeks, and are presented accordingly. Short-term 3-d experiments were performed in both stagnant and flowing conditions whereas the long-term 2-week experiments were only conducted in a stagnant condition. The 2-week experiments were meant to identify if there were any long-term changes in the percentage of the water-wetted area due to the hydrophilicity of the carbon steel. Stagnant conditions refer to the environment in a glass cell where the vapor transport is dominated by natural convection. Flowing conditions refer to the condensing tube through which the vapor phase is forced to flow along.

3.2.1 | Short-Term Exposure (3 D)

Baseline experiments (pure water system)—Figure 8 illustrates the corrosion rates as a function of WCR in both stagnant and flowing conditions. The results from both systems indicated that corrosion rates increased with WCR which is in good agreement with previous observations.[7,33] Higher WCR enhances the replenishment rate of freshly condensed water maintaining the corrosivity of the environment. In addition, at the lower/medium condensation rates (over the range of water condensation rates tested in this study), the corrosion rate under flowing conditions was higher than that of the stagnant condition.

SEM images show the morphology of the corrosion product layer as depicted in Figure 9. No $FeCO_3$ was observed in the stagnant condition (Figure 9[a]) whereas a layer of $FeCO_3$ precipitated under the flowing condition (Figure 9[b]). This could

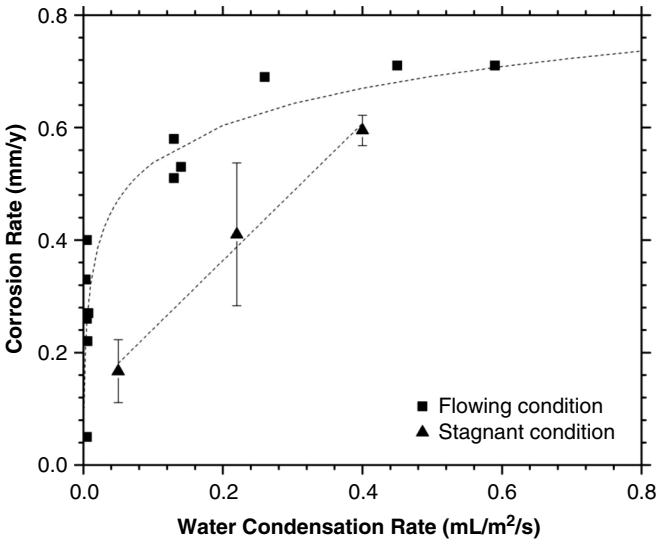

FIGURE 8. *Variations of weight loss corrosion rates with water condensation rates in a water condensation environment.*

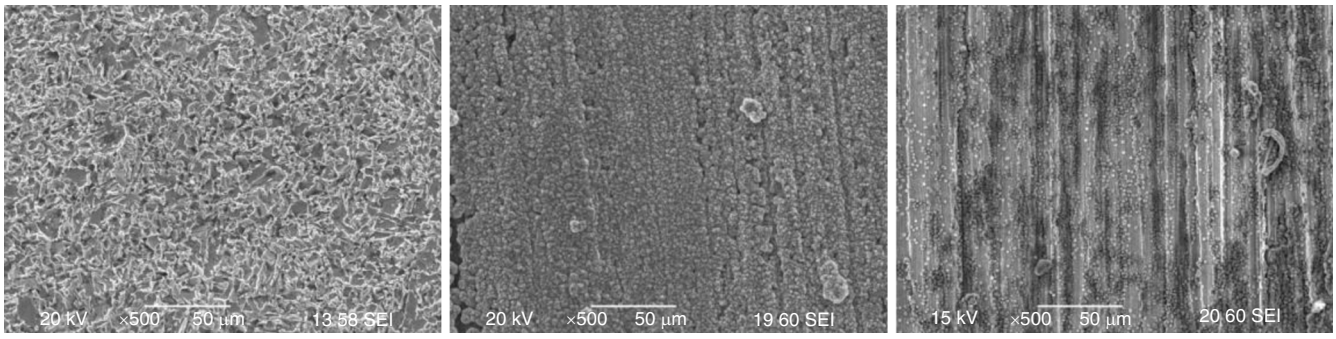

FIGURE 9. *SEM images of specimens exposed to water condensation at different vapor and cooling temperatures (T_v and T_c, respectively); (a) T_v/T_c = 50°C/30°C, 88 kPa pCO_2, 3 d exposure and WCR = 0.22 mL/m^2/s, stagnant condition, (b) T_v/T_c = 63°C/37°C, 77 kPa pCO_2, 3 d exposure and WCR = 0.45 mL/m^2/s, flowing condition, and (c) T_v/T_c = 20°C/18°C, 96 kPa pCO_2, 3 d exposure and WCR = 0.005 mL/m^2/s, flowing condition.*

be due to slow $FeCO_3$ precipitation kinetics as the specimen temperature under the stagnant condition was 7°C lower than those under the flowing condition. Long-term experiments may be required to elucidate the protectiveness of the $FeCO_3$ layer formed under the flowing condition.

Nonetheless, the surface temperature is not the only parameter controlling the precipitation of $FeCO_3$. Figure 9(c) shows that WCR also strongly influences the $FeCO_3$ precipitation even at extremely low surface temperature of 18°C. In this case, extremely low WCR (0.005 mL/m^2/s) led to the slow growth of water droplets allowing the buildup of ferrous ions leading to $FeCO_3$ supersaturation and consequent precipitation.

3D surface profilometry analysis shows that the steel was uniformly corroded when exposed to water condensation, as illustrated in Figures 10(a) and (b). Though the 3D image shown in Figure 10 is related to a stagnant condition, uniform corrosion was also observed for the specimen tested under the flowing condition. No localized corrosion is expected to occur in sweet TLC in a short-term corrosion experiment. Singer, et al., found no localized corrosion in their 2-d experiments even with acetic acid present up to 1,040 ppm.[34] Long-term experiments and highgas temperatures have been shown to be necessary for pits to grow.[4]

Co-condensation environments—Figure 11 compares the corrosion rates in the absence and presence of n-heptane

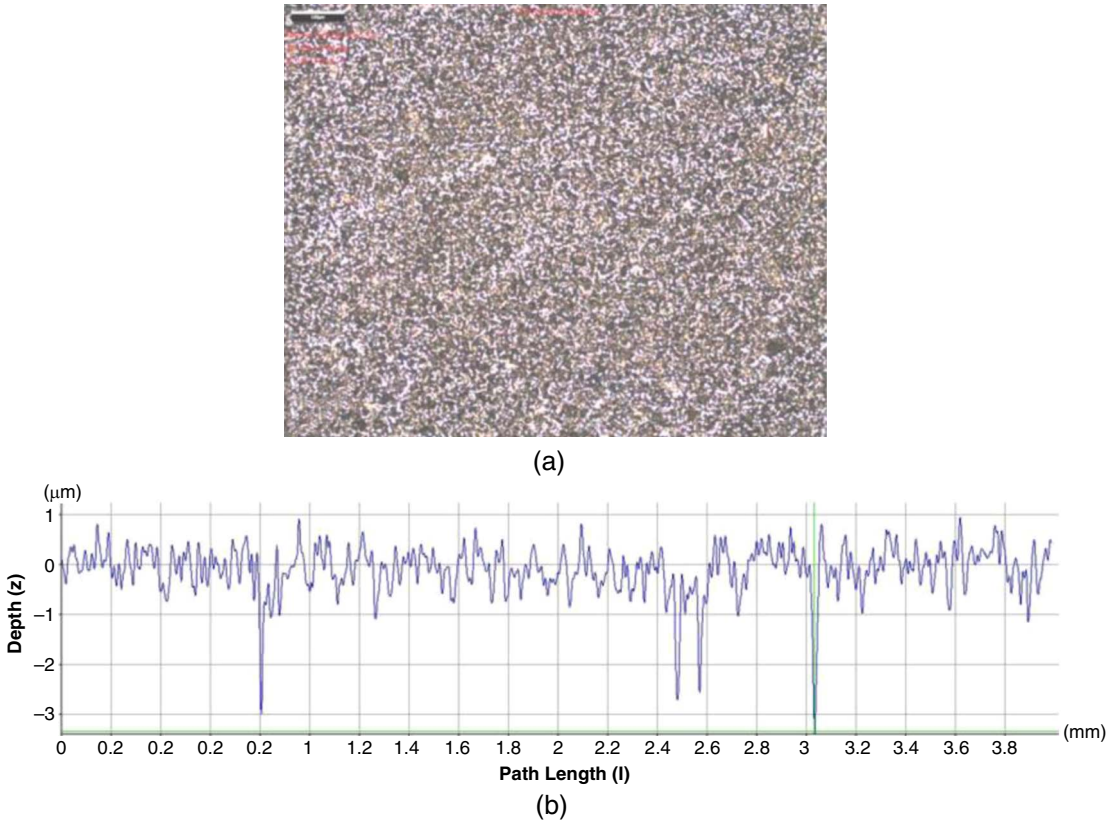

FIGURE 10. *Surface topography of specimen exposed to water condensation (vapor and cooling temperature of 50°C and 30°C, respectively. 88 kPa pCO_2, 3 d exposure and WCR = 0.22 mL/m^2/s, stagnant condition); (a) optical image and (b) depth profile analysis.*

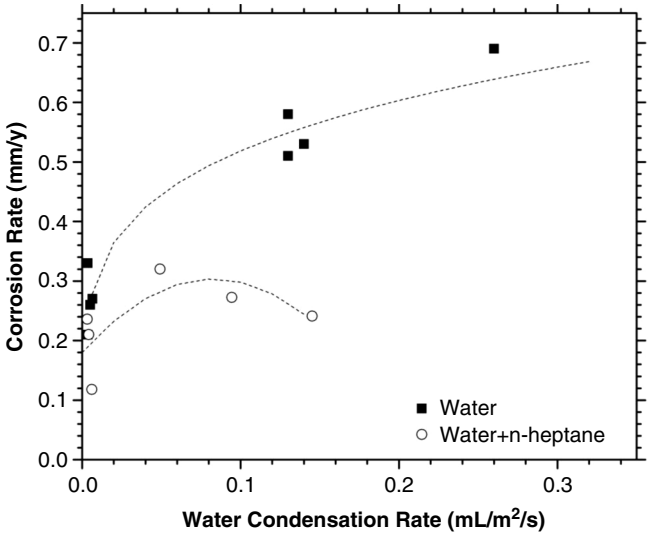

FIGURE 11. *Corrosion rates in the absence and presence of n-heptane co-condensation as a function of water condensation rate and under flowing condition (T_v = 18°C–50°C, 69 kPa–97 kPa pCO_2, 3 d exposure).*

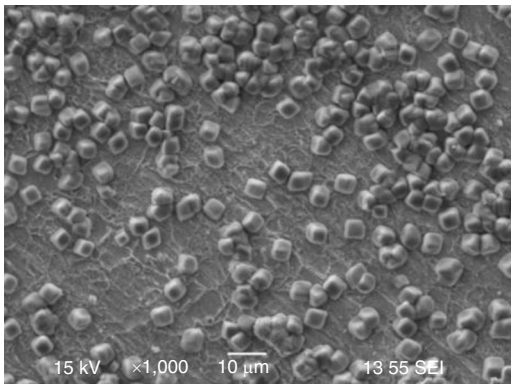

(a)

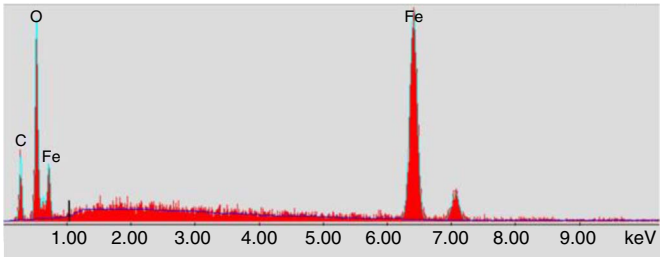

(b)

FIGURE 12. *SEM image and EDS spectrum of specimen exposed to co-condensation. Vapor and cooling temperature of 50°C and 30°C, respectively, 69 kPa pCO_2, 3 d exposure and water and n-heptane condensation rate = 0.19 mL/m²/s and 1.21 mL/m²/s, respectively (stagnant condition).*

under the flowing condition. Because the WCR is the primary parameter determining TLC, the corrosion rate was solely compared as a function of WCR, not the total condensation rate. It was found that in the absence of n-heptane, the corrosion rate increased with WCR as reported previously. However, no significant change in corrosion rate with respect to WCR was observed in the presence of n-heptane, especially above 0.05 mL/m²/s. In other words, the corrosion rate became less dependent on WCR in co-condensation scenarios.

Further analysis using SEM and EDS revealed that $FeCO_3$ precipitated in all co-condensation experiments even in the conditions where it was not found in the pure water environment. For instance, Figure 12 presents the SEM image and EDS spectrum of the specimen exposed to co-condensation under a stagnant condition for 3 d at vapor temperature (T_v) = 50°C and surface temperature (T_s) = 30°C and a WCR of 0.19 mL/m²/s. $FeCO_3$ crystals can be observed and their composition is confirmed by EDS analysis. It is observed that these crystals are not uniformly distributed and do not fully cover the underlying steel. On the contrary, at the same T_v and T_s, no $FeCO_3$ was detected in the pure water system as shown earlier in Figure 9. This suggests that the water chemistry, especially $FeCO_3$ saturation level, within the condensed liquid on the steel specimen in the co-condensation scenario differed from that in the pure water system. In this scenario, the condensed water had a higher concentration of ferrous ions and a higher pH. A detailed discussion about the effect of co-condensation on the water chemistry of the condensed water will be presented at the end of this manuscript.

Figure 13 shows the surface profilometry of the steel specimen after removing the corrosion products. In the presence of co-condensation, large areas exhibited extensive corrosion while others seemed relatively intact even with polishing marks visible. This shows that the two liquids, i.e., corrosive and noncorrosive, were simultaneously present in different areas of the steel specimen. It is certain that the less corroded areas correspond to the heptane-wetted area whereas the more corroded areas were wetted with water. In fact, the presence of n-heptane segregated water into smaller droplets. It is evident from the microscopic image (Figure 13[a]) that the coalescence of water droplets did not fully replace n-heptane. n-Heptane was still on the steel surface but probably in a small amount and could be identified by neither electrical conductivity measurement nor visual observation. As it was mentioned earlier, this is due to the stronger affinity (the hydrophilic behavior) of the carbon steel surface to water. The depth difference between the corroded and non-corroded (less corroded) area was approximately 2.5 µm which is equivalent to a penetration rate of 0.3 mm/y, which is very close to the WL corrosion rate (see Figure 10), suggesting that most of the surface was wetted by water droplets separated by a thin layer of n-heptane.

Additionally, as shown in Figure 14, the diameters of the water droplets condensing on the specimen surface appeared to be related to WCR. When the condensation rate of water was relatively high, water droplets readily coalesced and were as large as 5 mm in diameter. With very low condensation rates, water droplets had much smaller diameters with values ranging from 0.1 mm to 0.5 mm.

3.2.2 | Long-Term Exposure (2 Weeks)

n-Heptane was shown to segregate water droplets in short-term experiments, but it is important to verify if this observation stays true after a longer exposure time. Therefore, the exposure time was extended to 2 weeks to identify if water would eventually occupy the entire surface due to the hydrophilicity of the carbon steel.

Figure 15 presents the SEM image and the EDS spectrum of the surface of the specimen exposed to water condensation at

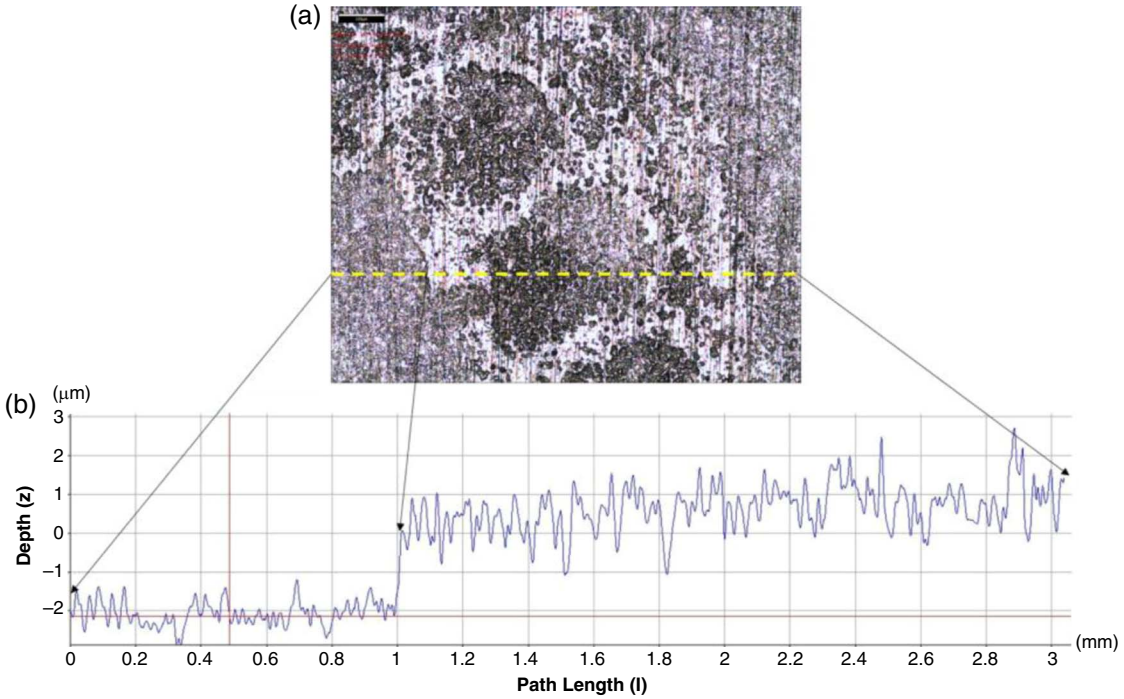

FIGURE 13. *3D surface profilometry of specimen exposed to co-condensation under stagnant condition (T_v/T_c = 50°C/35°C) after removing the corrosion products; (a) optical image and (b) depth profile analysis.*

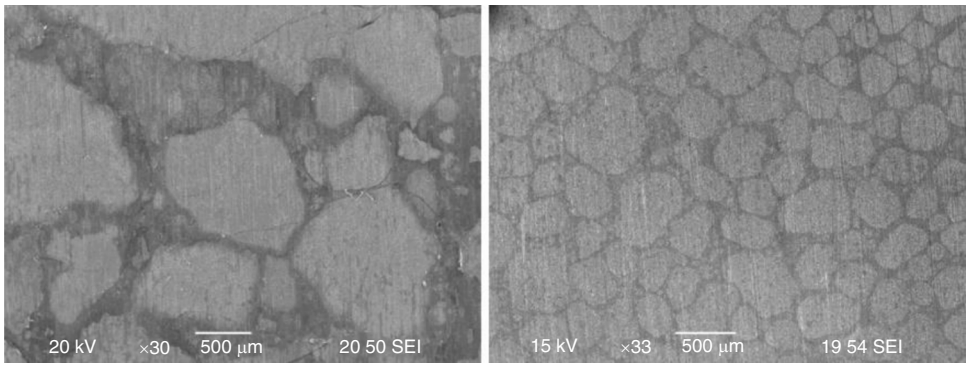

FIGURE 14. *Surface morphology of specimens exposed to different condensation rates (under flowing condition), vapor and cooling temperature (T_v and T_c, respectively) showing different droplet sizes; (a) T_v/T_c = 40.5°C/15.7°C (water and n-heptane condensation rate = 0.1 mL/m^2/s and 0.65 mL/m^2/s, respectively) and (b) T_v/T_c = 19.3°C/17.6°C (water and n-heptane condensation rate = 0.003 mL/m^2/s and 0.022 mL/m^2/s, respectively).*

a rate of 0.22 mL/m^2/s for 2 weeks under the stagnant condition. No $FeCO_3$ was observed on the surface. This was expected as the experimental conditions were not thermodynamically favorable for $FeCO_3$ precipitation, i.e., low temperature and low pCO_2. The EDS results show that the majority of the surface is composed of iron with some other alloying elements present at lower concentrations. In conjunction with the surface morphology, it is concluded that a nonprotective iron carbide, Fe_3C was likely present as a by-product of the corrosion process. The surface was uniformly corroded as depicted with 3D surface profilometry in Figure 16. It can be observed that the surface became rougher compared to the short-term experiment (Figure 10) indicating that the specimen was uniformly corroded to a greater extent.

Similar to what was observed in the short-term experiments, the SEM image of the specimen in the co-condensation scenario revealed areas resembling water droplets of different sizes, ranging from 100 μm to 2 cm (Figure 17[a]). The EDS spectrum of crystal-like particles showing the dominant peaks of Fe, C, and O suggests the presence of $FeCO_3$ (Figure 17[d]). At the border of a water droplet, the SEM backscattered image (Figure 17[c]) shows a dense corrosion product on the outside edge. Further into the center of the water droplet, $FeCO_3$ sparsely precipitated and the underlying base metal was exposed. After cleaning the surface, the area underneath the droplet was found to be corroded uniformly confirming that the droplet was made of water. As observed in a short-term experiment in the co-condensation scenario, some areas were not corroded even when extending the exposure time to 2 weeks suggesting that a microscopic fraction of the surface was always occupied by n-heptane which resulted in a long-term segregation of water droplets.

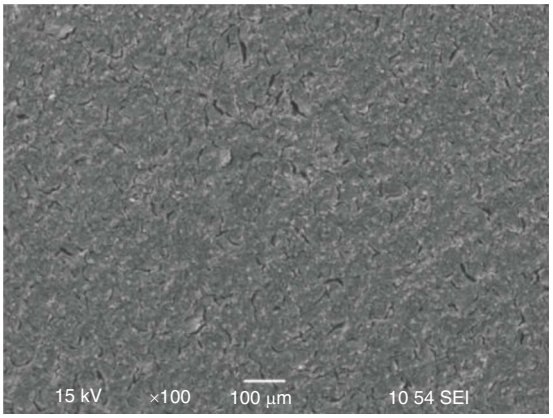

(a)

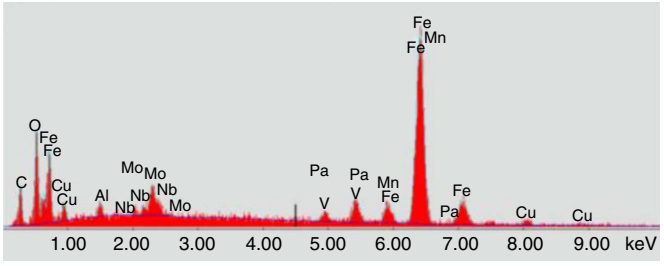

(b)

FIGURE 15. *SEM image and EDS spectrum of the specimen exposed to water condensation for 2 weeks. (WCR = 0.22 mL/m^2/s), stagnant condition.*

The variation of weight loss corrosion rates with time between two condensation scenarios are compared in Table 3. In the absence of hydrocarbons, the weight-loss corrosion rate increased by 68%, from 0.50±0.13 mm/y to 0.84±0.01 mm/y when the exposure time was increased from 3 d to 13 d. The increase in corrosion rate of carbon steel with time could be attributed to the galvanic coupling between Fe_3C and the base metal, where Fe_3C acts as the extra cathodic site, as previously reported.[35-37] When n-heptane was present, the corrosion rate was not dependent on the exposure time. The weight-loss corrosion rates were 0.16±0.12 mm/y and 0.19±0.03 mm/y for the 3 d and 13 d exposure, respectively. While the mean value slightly increased, the standard deviation of the 3 d exposure was large thus indicating no measurable difference between the corrosion rates of the 3 d and 13 d exposure.

Table 3 also shows the maximum penetration depth and rate, respectively. The maximum penetration depth, obtained from the bottommost areas from the 3D surface profiles, increased as the exposure time increased. The maximum penetration rates were relatively constant with time in both scenarios.

3.3 | Discussion: The Change in Water Chemistry of Condensed Water During Hydrocarbon Co-Condensation and the Effect on Corrosion

It becomes evident that the change in the water chemistry of condensed water due to the segregation of water droplets could be regarded as the primary cause of the corrosion rate reduction in the co-condensation environment. To illustrate the change in water chemistry due to co-condensation, speciation calculation of aqueous species commonly encountered in

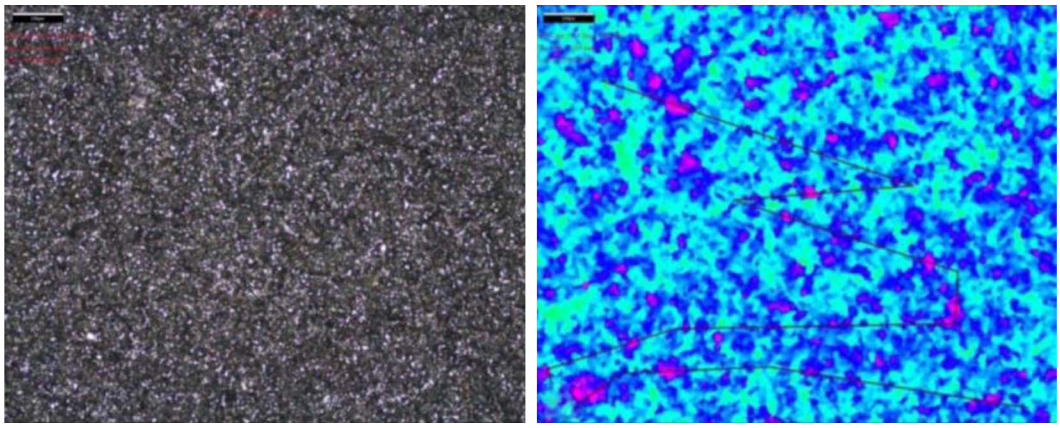

(a) (b)

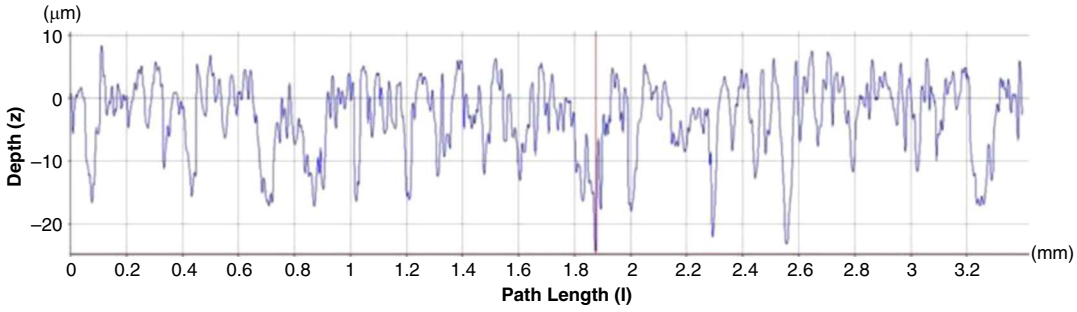

(c)

FIGURE 16. *Surface topography of specimen after the removal of corrosion product exposed to condensation of water only for 2 weeks (WCR = 0.22 mL/m^2/s), stagnant condition.*

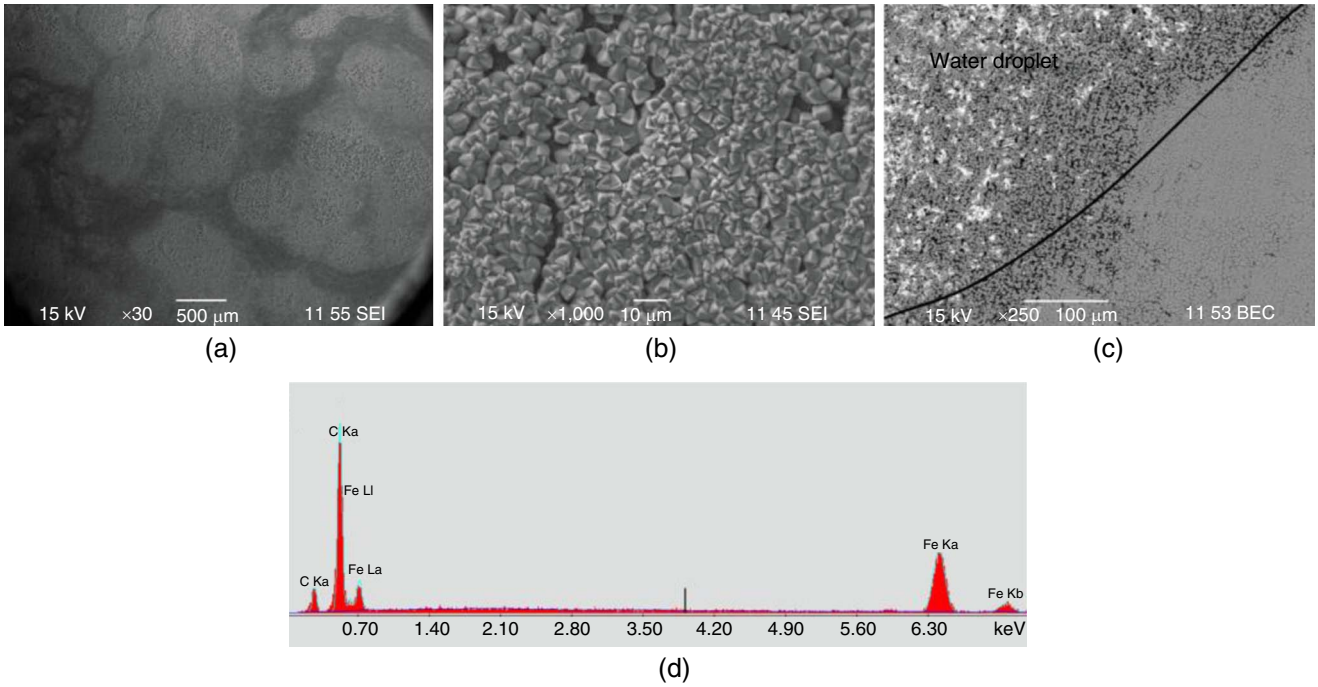

FIGURE 17. *SEM images of specimen exposed to the co-condensation of water and n-heptane for 2 weeks (water and n-heptane condensation rate = 0.19 mL/m^2/s and 1.21 mL/m^2/s, respectively); (a) low magnification image showing the overall area of the specimen, (b) close-up SEM image of the $FeCO_3$ crystals, (c) SEM image at the border of water droplet showing the distribution of $FeCO_3$, and (d) and EDS spectrum of the $FeCO_3$ crystals shown in (b).*

Table 3. *Comparison of Weight-Loss Corrosion Rates, Maximum Pit Depth, and Maximum Pitting Rate of Carbon Steel Exposed to Condensation of Water and Water/n-Heptane for 3 d and 13 d*[(A)]

Parameters	Water		Water/n-Heptane	
	3 d	13 d	3 d	13 d
Weight Loss Corrosion Rate (mm/y)	0.5±0.13	0.84±0.01	0.16±0.12	0.19±0.03
Maximum Pit Depth (µm)	6.6±0.5	29.6±2.2	5.1±0.9	19.7±1.3
Maximum Pitting Rate (mm/y)	0.80±0.08	0.83±0.06	0.61±0.11	0.55±0.04

(A) T_v and T_c were 50°C and 30°C, respectively.

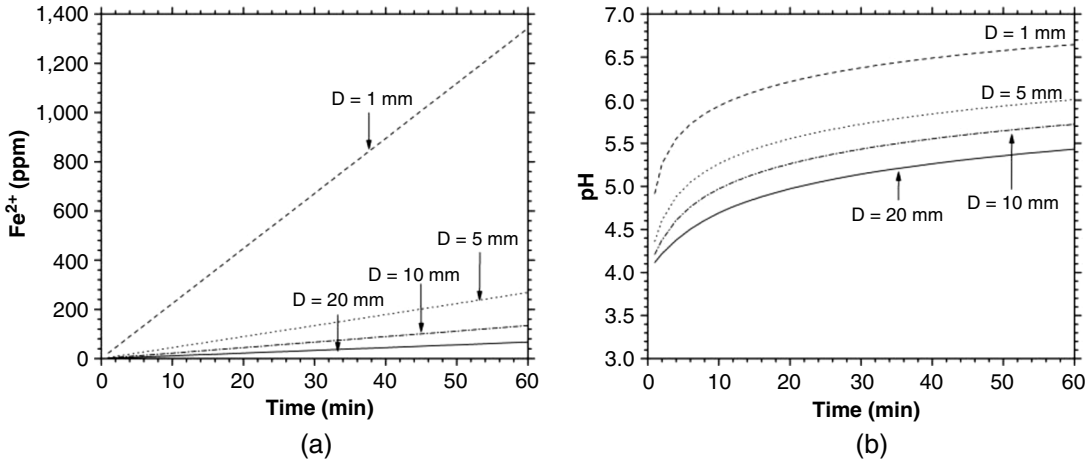

FIGURE 18. *(a) Calculated ferrous ion accumulation and (b) the change in pH within water droplet of different diameters (D) vs. time (common parameter for calculation: $T_{surface}$ = 50°C, total pressure = 101.3 kPa, and corrosion rate = 0.5 mm/y).*

CO_2 corrosion was performed. Chemical equilibrium for reactions in CO_2 corrosion has been established and summarized elsewhere.[37] As water droplets are segregated into smaller droplets, the surface area to volume (A/V) ratio becomes greater. If the water droplet is assumed to have a hemispherical shape, the A/V ratio increases from 150 m^{-1} to 3,000 m^{-1} when the diameter decreases from 2 cm to 1 mm. It was proposed that the precipitation rate of $FeCO_3$ is a function of A/V ratio.[38] Additionally, the water chemistry within different size droplets evolved differently over time due to the different A/V ratios. For instance, assuming the same initial corrosion rate of 0.5 mm/y, the Fe^{2+} concentration accumulated within different water droplet sizes varies, as shown in Figure 18(a). Consequently, the concentration of H^+ ions and the pH within the droplet change. As shown in Figure 18(b), the pH in smaller droplets becomes higher than that in larger droplets, which would lead to a less corrosive solution. As a result, higher concentrations of ferrous ion and subsequently higher pH could be expected, i.e., the situation favorable for $FeCO_3$ precipitation.

In wet gas transportation pipelines, many hydrocarbons in addition to n-heptane could also be condensable. Nonetheless, a similar condensation pattern to that of water/n-heptane may be expected. The condensed liquids, water, and hydrocarbons are immiscible and thus water droplets are segregated. However, further investigation into the co-condensation rates of water and various hydrocarbons is crucial to better understand the process of water condensation, water droplets segregation, and consequently corrosion.

CONCLUSIONS

The influence of co-condensation of water and n-heptane on TLC was investigated. The study was done in two parts, i.e., the first part focusing on the co-condensation process and the second part on the corrosion process. The results show that:

- Water alone condenses in a different fashion from n-heptane (dropwise vs. film-wise due to surface tension). When both species condense simultaneously, n-heptane seems to retard the coalescence of nearby water droplets, segregating water droplets into smaller droplets.
- The segregation caused by the co-condensation of n-heptane leads to the change in water chemistry within water droplets which was confirmed by the existence of a protective $FeCO_3$ only in the co-condensation scenario.
- As a result, the TLC rate tends to decrease in the co-condensation scenario in comparison to the water-only system and appears to be less dependent on WCR.

ACKNOWLEDGMENTS

The authors would like to acknowledge the technical guidance and financial support provided by the sponsor companies of the Top of the Line Corrosion Joint Industry Project at the Institute of Corrosion and Multiphase Technology, Ohio University: Total, BP, ConocoPhillips, Chevron, Saudi Aramco, Occidental Oil Company, ENI, and PTTEP.

References

1. Y. Gunaltun, D. Supriyatman, J. Achmad, "Top of Line Corrosion in Multiphase Gas Lines. A Case History," *CORROSION 1999*, paper no. 99036 (Houston, TX: NACE, 1999).
2. Y. Gunaltun, S. Punpruk, M. Thammachart, P. Tanaprasertsong, "Worst Case Top of the Line Corrosion: Cold Spot Corrosion," *CORROSION 2010*, paper no.10097 (Houston, TX: NACE, 2010).
3. R. Paillassa, M. Dieumegard, M.M. Estavoyer, "Corrosion Control in The Gathering System at LACQ Sour Gas Field," *2nd International Congress on Metallic Corrosion*, 1963, p. 410-417.
4. M. Singer, D. Hinkson, Z. Zhang, H. Wang, S. Nešić, *Corrosion* 69, 7 (2009): p. 719-735.
5. D. Hinkson, Z. Zhang, M. Singer, S. Nešić, *Corrosion* 66, 4 (2010): p. 045002 to 045002-08.
6. M. Singer, A. Camacho, B. Brown, S. Nešić, *Corrosion* 67, 8 (2011): p. 085003-1 to 085003-16.
7. Y.M. Gunaltun, D. Larrey, "Correlation of Cases of Top of the Line Corrosion with Calculated Water Condensation Rates," *CORROSION 2000*, paper no. 00071 (Houston, TX: NACE, 2000).
8. S.B.S. Anuar, M.C. Ismail, P.B. Raja, N.A.B.A. Rahman, *ARPN J. Eng. Appl. Sci.* 11, 20 (2016): p. 12058-12063.
9. F. Rozi, H. Mohebbia, M.C. Ismail, S. Kakooeia, M. Ahmadia, A. Aghasadeghib, A. Aghasadeghic, *Corros. Eng. Sci. Technol.* 53, 6 (2018): p. 1-5.
10. M.M. Islam, T. Pojtanabuntoeng, R. Gubner, *Corros. Sci.* 111 (2016): p. 139-150.
11. S. Qian, Y.F. Cheng, J. Nat. Gas Sci. Eng. 68 (2019): p. 102921.
12. T.R. Anderson, A.M.K. Halvorsen, A. Valle, G.P. Kojen, A. Dugstad, "The Influence of Condensation Rate and Acetic Acid Concentration on TOL Corrosion in Multiphase Pipelines," *CORROSION 2007*, paper no. 07312 (Houston, TX: NACE, 2007).
13. B.F.M. Pots, E.L.J.A. Hendriksen, "CO_2 Corrosion Under Scaling Conditions: The Special Case of Top of Line Corrosion in Wet Gas Pipelines," *CORROSION 2000*, paper no. 00031 (Houston, TX: NACE, 2000).
14. C. De Waard, U. Lotz, D.E. Milliams, *Corrosion* 47, 12 (1991): p. 976-985.
15. Z. Zhang, D. Hinkson, M. Singer, H. Wang, S. Nešić, *Corrosion* 63, 11 (2007): p. 1051-1062.
16. F. Ayello, W. Robbins, S. Richter, S. Nešić, "Crude Oil Chemistry Effects on Inhibition of Corrosion and Phase Wetting," *CORROSION 2011*, paper no. 11060 (Houston, TX: NACE, 2011).
17. L.D. Paolinelli, A. Rashedi, J. Yao, M. Singer, *Chem. Eng. Sci.* 183 (2018): p. 200-214.
18. F. Ayello, "Crude Oil Chemistry Effects on Corrosion Inhibition and Phase Wetting in Oil-Water Flow" (Ph.D. thesis diss., Ohio University, 2010).
19. U. Lotz, L. van Bodegom, C. Ouwehand, *Corrosion* 47, 8 (1991): p. 635-644.
20. M. Simon-Thomas, K.G. Jordan, S.E. Lorimer, P.B. Hebert, "Inhibition of Sweet Corrosion of Subsea Flowlines," *CORROSION 1998*, paper no. 57 (Houston, TX: NACE, 1998).
21. S.H. Bernhardt, J.J. Sheriden, J.W. Westwater, *AIChE J.* 68, 118 (1972): p. 21-37.
22. W. Akers, M. Turner, *AIChE J.* 8, 5 (1962): p. 587-589.
23. E. Reimann, J. Mitrovic, *Heat Technol.* 17, 2 (1999): p. 71-79.
24. J. Kim, D. Webb, *Chem. Eng. Res. Des.* 67 (1989): p. 87-95.
25. O. Tutkun, *Chem. Eng. Process.* 33 (1994): p. 429-436.
26. O. Fumimaru, K. Shuji, M. Tokuro, *Int. J. Heat Mass Transfer* 31, 2 (1988): p. 245-250.
27. T. Pojtanabuntoeng, M. Singer, S. Nešić, "Water/Hydrocarbon Co-Condensation and The Influence on Top of the Line Corrosion," *CORROSION 2011*, paper no. 11330 (Houston, TX: NACE, 2011).
28. J. Cai, C. Li, X. Tang, F. Ayello, S. Richter, S. Nešić, Chem. Eng. Sci. 73 (2012): p. 334-344.
29. C. Li, "Effect of Corrosion Inhibitor on Water Wetting and Carbon Dioxide Corrosion in Oil-Water Two-Phase Flow" (Ph.D. thesis diss., Ohio University, 2009).
30. ASTM G1 (latest edition), "Standard Practice for Preparing, Cleaning, and Evaluating Corrosion Test Specimens" (West Conshohocken, PA: ASTM International, 2017).
31. T. Pojtanabuntoeng, M. Singer, S. Nešić, "Top of the Line Corrosion in the Presence of Hydrocarbon Co-Condensation in Flowing Condition," *CORROSION 2012*, paper no. 01534 (Houston, TX: NACE, 2012).
32. X. Tang, S. Richter, S. Nešić, "Study of Wettability of Different Mild Steel Surface," in *17th International Corrosion Congress*, paper no. 3109, Las Vegas, NV, 2008.
33. H. Qin, L. Xu, W. Chang, M. Lu, L. Zhang, "Top of the Line Corrosion Under Low Temperature and High Condensation Rate Conditions," *CORROSION 2011*, paper no. 11328 (Houston, TX: NACE, 2011).

34. M. Singer, S. Nešić, Y. Gunaltun, "Top of the Line Corrosion in Presence of Acetic Acid and Carbon Dioxide," *CORROSION 2004*, paper no. 04377 (Houston, TX: NACE, 2004).
35. J. L. Crolet, N. Thevenot, S. Nešić, *Corrosion* 54, 3 (1998): p. 194-203.
36. F. Farelas, M. Galicia, B. Brown, S. Nešić, H. Castaneda, *Corros. Sci.* 52, 2 (2010): p. 509-517.
37. S. Nešić, W. Sun, "Corrosion in Acid Gas Solutions," in *Shrier's Corrosion* (Amsterdam, Netherlands: Elsevier Science, 2010), p. 1270-1298.
38. W. Sun, S. Nešić, *Corrosion* 64, 4 (2008): p. 334-346.